Available online at www.sciencedirect.com
SCIENCE DIRECT®
Journal of Nuclear Materials 351 (2006) 228–240
journal of nuclear materials
www.elsevier.com/locate/jnucmat

Microstructural development in cubic silicon carbide during irradiation at elevated temperatures

Y. Katoh [a,*], N. Hashimoto [a], S. Kondo [b], L.L. Snead [a], A. Kohyama [b]

[a] *Metals and Ceramics Division, Oak Ridge National Laboratory, 1 Bethel Valley Road, P.O. Box 2008, MS-6138, Oak Ridge, TN 37831-6138, USA*
[b] *Institute of Advanced Energy, Kyoto University, Gokasho, Uji, Kyoto 611-0011, Japan*

Abstract

Microstructural development in chemically vapor-deposited (CVD) high-purity beta-SiC during neutron and self-ion irradiation at elevated temperatures was studied. The CVD SiC samples were examined by transmission electron microscopy following neutron irradiation to $4.5–7.7 \times 10^{25}$ n/m^2 ($E > 0.1$ MeV) at 300 and 800 °C and 5.1 MeV Si^{2+} ion irradiation up to ~200 dpa at 600–1400 °C. The evolution of various irradiation-produced defects including black spot defects, dislocation loops, network dislocations, and cavities was characterized as a function of irradiation temperature and fluence. It was demonstrated that the black spot defects and small dislocation loops continue to dominate at relatively low temperatures (<~800 °C), whereas they grow into Frank faulted loops and finally develop into dislocation networks at a higher temperature (1400 °C). Substantial cavity formation on grain boundaries and stacking faults was confirmed after ion irradiation at 1400 °C. These observations were discussed in relation with the known irradiation phenomena in SiC, such as low temperature swelling and cavity swelling.

1. Introduction

Silicon carbide (SiC) and SiC-based ceramic composites are both promising materials for various structural and functional components in nuclear energy systems. Chemically vapor deposited (CVD) SiC has been considered as the pressure vessel material for high temperature gas-cooled reactor (HTGR) fuel particles [1] and the solid matrix material of fuel blocks for the gas fast reactors (GFR). SiC fiber-reinforced SiC-matrix composites are the advanced options for the control rod sleeves and the guide tubes materials in very high temperature reactors (VHTR) [2]. Moreover, some of the GFR core concepts assume the SiC/SiC composite to be a viable material for the extensive use, for example, as the fuel pin cladding [3,4]. For fusion reactors, the use of SiC/SiC composites for primary structures is envisioned in a variety of gas-cooled and liquid metal-cooled blanket concepts [5,6]. Some of the proposed test blanket module (TBM) designs for the international thermonuclear experimental reactor (ITER) utilize SiC and/or SiC/SiC

* Corresponding author. Tel.: +1 865 576 5996; fax: +1 865 241 3650.
E-mail address: katohy@ornl.gov (Y. Katoh).

0022-3115/$ - see front matter © 2006 Elsevier B.V. All rights reserved.
doi:10.1016/j.jnucmat.2006.02.007

composites as the materials for flow channel insert (FCI) [7] and solid breeding pebble containers.

All the materials mentioned above consisted primarily of polycrystalline beta-phase (or cubic) SiC that has the 3C crystallographic structure. The primary benefit of using beta-SiC and its composites for nuclear applications is the potential lack of severe effects of neutron irradiation, in addition to other well-known advantages of SiC such as the retention of strength and chemical inertness up to very high temperatures and the inherent low activation/low decay heat properties. For monolithic beta-SiC, strength retention after neutron irradiation to $\sim 2 \times 10^{26}$ n/m^2 at 740 °C has been reported by Price and Hopkins [8]. Moreover, strengthening and/or toughening of beta-SiC by neutron irradiation to 1×10^{23}–8×10^{25} n/m^2 ($E > 0.1$ MeV) at temperatures of 80–1050 °C are likely according to recent reports [9–13]. On the contrary, Dienst reports a substantial degradation of flexural strength of CVD SiC beyond the neutron fluences over 1×10^{26} n/m^2 at 400–600 °C [14–16]. For composites with the matrices and the reinforcing fibers both made of (near-) stoichiometric beta-SiC, no degradation in the ultimate flexural strength has been reported after neutron irradiation up to $\sim 8 \times 10^{25}$ n/m^2 at 300–800 °C [17–20].

In addition to the fracture strength modifications, a variety of irradiation effects in SiC has been reported. They are far from well understood in terms of physical mechanism and microstructural processes. For example, the irradiation-induced toughening of CVD SiC is often observed [13], but the responsible microstructural defects and the mechanism have not been clarified.

The low temperature swelling is a well known irradiation-induced phenomenon for crystalline SiC [21–24]. During irradiation at temperatures below ~1000 °C, SiC undergoes isotropic volume expansion that initially increases with the fluence and eventually saturates at temperature-dependent values [25]. Such characteristics have been utilized for the operation temperature estimation of test capsules in nuclear reactors. However, in spite of the extensive phenomenological studies for temperature monitor applications, microstructural defects responsible for low temperature swelling have not been identified. Thermal conductivity degradation, which has also been extensively studied [26–28] and appeared to be strongly correlated with the magnitude of low temperature swelling [29], has not been linked to the primary contributing defects. The difficulty in identifying the mechanisms for the low temperature swelling and the thermal conductivity degradation could be attributed to the complex nature of point defects in the ceramic compound, the lack of defect clusters easily resolvable by transmission electron microscopy (TEM) for irradiation at temperatures below ~800 °C, the lack of reliable energetics for the point defects, and the estimated similar contributions from the various defect species [30–32].

Other important irradiation phenomena in SiC include cavity swelling and irradiation creep. Cavity production in beta-SiC by neutron irradiation has been reported at temperature above 1250 °C [33]. However, the phenomenological understanding of cavity swelling in SiC has not been incomprehensive and the driving mechanism has not been discussed to the best of our knowledge. Also, very little is known about the irradiation creep phenomena and the mechanisms, in spite of the potential extreme importance of the irradiation creep issues for the nuclear thermostructural applications [34–36]. In order to obtain insights to the kinetics of both cavity swelling and irradiation creep, fundamental understanding of the dislocation evolution during irradiation has to be gained.

This work is motivated to advance the fundamental understanding of microstructural evolution in polycrystalline beta-SiC during irradiation, in order to aid addressing its various irradiation phenomena. Specifically, the microstructures after neutron and self-ion irradiations at relatively low temperatures were examined, primarily in relation to low temperature swelling. The cavity swelling and dislocation evolution during self-ion irradiation were also examined. The technique of self-ion irradiation was employed particularly for the purpose of studying microstructural evolution at very high temperatures, taking advantage of the versatility of target setup in ion irradiation experiments. Finally, mapping of the microstructural development in beta-SiC as a function of irradiation temperature and fluence was attempted. In addition to the nuclear applications, the obtained microstructural information is relevant to studies on SiC for applications in semiconductor and space industries, and accelerator facilities.

2. Experimental procedure

The material used was CVD SiC produced by Rohm and Haas Advanced Materials (Woburn,

Massachusetts), which is a high-purity (>99.9995% manufacturer-claimed purity) polycrystalline beta-SiC. The crystal grains in this material are columnar-shaped typical in the CVD-grown SiC. The column width is mostly 1–50 μ and approximately parallel to one of the {1 1 1} planes. The crystal grains are highly faulted with the typical stacking fault inter-distances of a few 100 nm.

Neutron irradiation was performed in the removable beryllium (RB) facility and the peripheral target position tubes of the high flux isotope reactor (HFIR) at the Oak Ridge National Laboratory (ORNL). Bend bar samples of CVD SiC were irradiated to 6.0×10^{25} n/m^2 ($E > 0.1$ MeV) at 300 °C and 4.5 and 7.7×10^{25} n/m^2 at 800 °C. Assuming that 1.0×10^{25} n/m^2 corresponds to 1 dpa in SiC, damage rate for the neutron irradiation was $\sim 5 \times 10^{-7}$ dpa/s. The irradiation temperature was maintained typically within ±20 °C of the designated temperature. Thin foil samples for microstructural examination were prepared by cutting with a low speed diamond saw, grinding with diamond paste, and ion milling with 3 keV argon ions in a Gatan Model 600 Duo Mill.

The self-ion irradiation was performed at the DuET multi-beam accelerator facility, Kyoto University [37,38]. The irradiation temperatures and the dose were 600–1400 °C and up to ~200 dpa, respectively. 5.1 MeV Si^{2+} ions were used and the damage rate was $\sim 1 \times 10^{-3}$ dpa/s at the depth of 1 μm. The temperature of individual specimens was monitored by infrared thermography that was calibrated in situ using a thermocouple, and was maintained within ±10 °C of the designated temperature. The ion beam flux distribution was monitored intermittently by a two-dimensional array of micro-Faraday cups. The conversion from beam flux to damage rate relied on the calculation using the TRIM-98 code and the sublattice-averaged displacement threshold energy of 35 eV [39]. The calculated profiles of the damage rate and the deposition rate of injected silicon ions are presented in Fig. 1. The ion-irradiated samples were made into cross-sectional thin foils through a focused ion beam (FIB) processing using <30 keV gallium ions.

The microstructural examination was carried out by using JEOL JEM-2000FX and JEM-2010ES-II transmission electron microscopes (TEM), both operated at 200 kV. The ion-irradiated specimens were examined in the areas typically 1000 nm from the irradiated surface, which is sufficiently distant from the surface during irradiation. The estimated concentration of deposited silicon ions is five atomic parts-per-million per dpa.

3. Results

Fig. 2(A) shows the microstructure of cubic SiC irradiated to 6.0×10^{25} n/m^2 at 300 °C, taken near

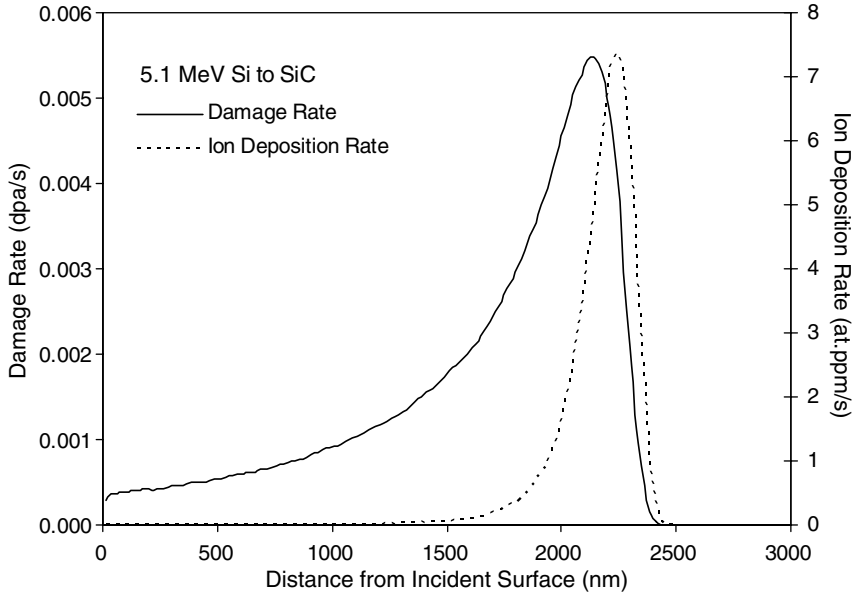

Fig. 1. Depth profile of displacement damage rate and ion deposition rate in SiC, during irradiation by 5.1 MeV Si^{2+} ions, calculated by TRIM-98 code assuming displacement threshold energy of 35 eV.

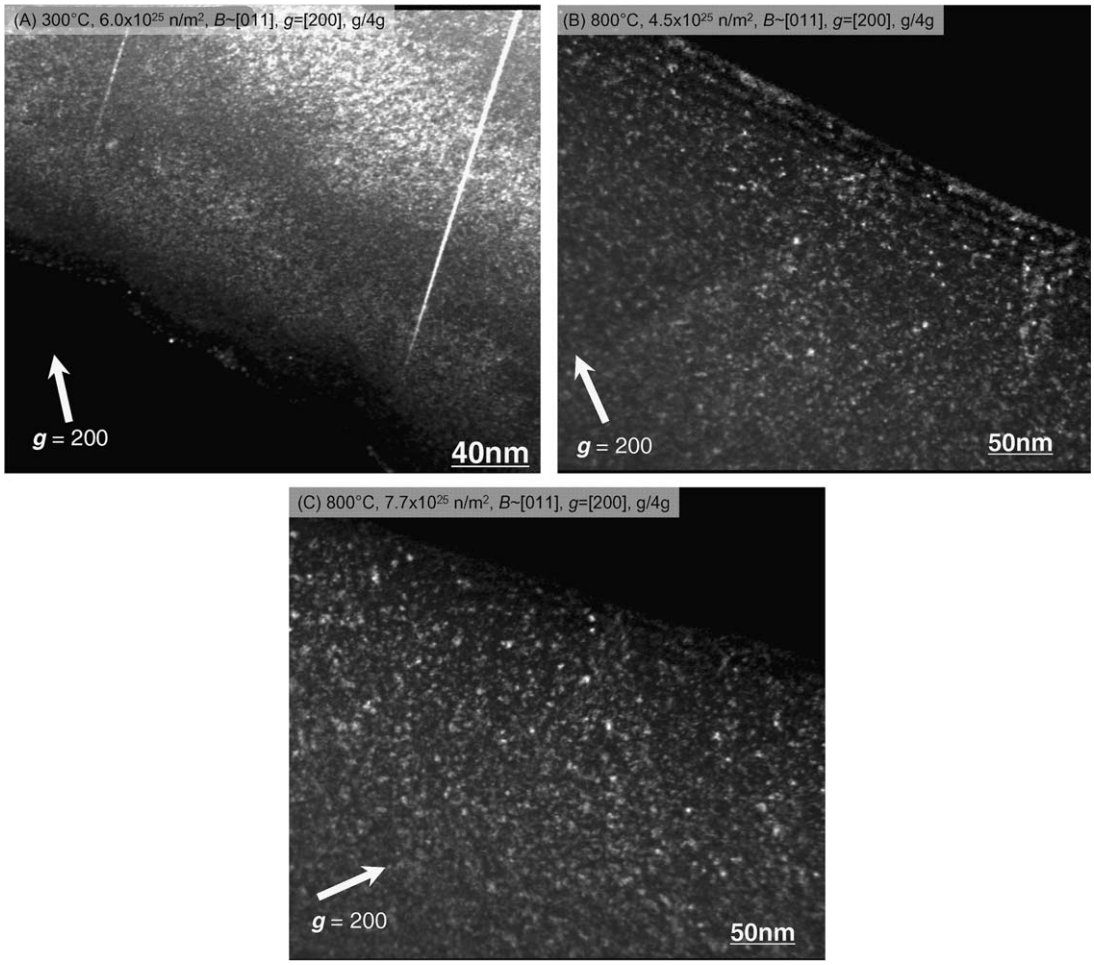

Fig. 2. Weak beam dark field images of the defect microstructures in neutron-irradiated cubic SiC. (A) 300 °C, 6.0×10^{25} n/m^2; (B) 800 °C, 4.5×10^{25} n/m^2; and (C) 800 °C, 7.7×10^{25} n/m^2.

a beam direction $B \sim [0\,1\,1]$ and with the diffraction vector g parallel to [2 0 0]. The only apparent microstructural feature added by the neutron irradiation was small clusters with a strain contrast, which were uniformly dispersed at a high density. These clusters appear as dark spots in a bright field image and are often called black spot defects or black dot defects. The mean size of the black spot defects estimated from the weak beam dark field images was smaller than 1 nm, whereas the density appeared to be 2.2×10^{24} m^{-3}. Result of the microstructural observation is summarized in Table 1.

Fig. 2(B) and (C) shows the weak beam dark field images of the samples irradiated to 4.5×10^{25} and 7.7×10^{25} n/m^2, respectively, at 800 °C. The imaging condition is identical with that in Fig. 1(A). At this temperature, many of the defect clusters appeared as or looked like dislocation loops and the rest appeared as the black spot defects. Irradiation-produced defects of other types, such as large dislocation loops and voids, were not found. A larger fraction of the defects was identified as loops at 7.7×10^{25} n/m^2 than at 4.5×10^{25} n/m^2. Therefore, it is likely that the small clusters appearing as black spot defects develop into dislocation loops as the neutron fluence increases. The defect size, averaged over the loop diameters and the black spot diagonals, increased from ~2.6 nm at 4.5×10^{25} n/m^2 to ~3.0 nm at 7.7×10^{25} n/m^2. Also, the total number density of the visible loops and black spot defects slightly increased from 2.6×10^{23} m^{-3} to 3.3×10^{23} m^{-3} as the neutron fluence increased.

In the electron diffraction patterns for the neutron irradiated samples, no satellite streaks were detected. Attempts to visualize the $\langle 1\,1\,1 \rangle$ streak images revealed only the stacking faults which had

Table 1
Microstructural data for irradiated cubic SiC

Irr. temp. (°C)	Dose ($\times 10^{25}$ n/m^2 or dpa)	Black spot/loops			Cavities	
		Type	Density (m^{-3})	Radius[a] (nm)	Density (m^{-3})	Radius (nm)
Neutron (0.5×10^{-6} dpa/s, HFIR, ORNL)						
300	6.0	Black spots	2.2×10^{24}	<0.5	Not detected	
800	4.5	Mix	2.6×10^{23}	1.3	Not detected	
800	7.7	Mix	3.3×10^{23}	1.5	Not detected	
Ion ($\sim 1 \times 10^{-3}$ dpa/s, 5.1 MeV Si^{2+}, DuET, Kyoto University)						
600	10	Black spots	n/m[b]	n/m	Not detected	
800	10	Mix	n/m	2.2	Not detected	
1000	10	Loops	2.6×10^{23}	~2	$<1 \times 10^{20}$	1.6[c]
1400	10	Loops	2.3×10^{21}	~5	2.0×10^{22}[d]	~2.0
1400	30	Loops	2.3×10^{21}	12.0	1.3×10^{24}[d]	~2.0
1400	100	Loops	5.2×10^{21}	18.1	1.8×10^{24}[d]	~2.0

[a] 1/2 of the approximate mean size for the black spot defects.
[b] Not measured.
[c] Grain boundary cavities.
[d] Local number density of grain/twin boundary cavities.

been pre-existing in the as deposited material. Additionally, only a few loops produced at 800 °C appeared in the edge-on orientations in the $B = \langle 0\,1\,1 \rangle$ beam direction, whereas the 50% of the Frank faulted loops lying on $\{1\,1\,1\}$ family planes must appear edge-on. Therefore, the majority of the dislocation loops observed are not Frank loops.

An attempt was made to identify the loops' Burgers vector by examining the visibility of loops in several different reflection conditions. An example pair of the micrographs is presented in Fig. 3. In this case, loops which have a strong contrast with $g = [2\,0\,0]$ are not visible with $g = [1\,1\,\bar{1}]$. The other way around, loops clearly visible with $g = [1\,1\,\bar{1}]$ completely disappear with $g = [2\,0\,0]$. These loops most likely have Burgers vector parallel to $\langle 0\,1\,1 \rangle$ and presumably $a/2\langle 0\,1\,1 \rangle$ in this system. Also, some of the clusters with a strong contrast in a $B \sim [\bar{1}\,1\,2]$ and $g = [3\,1\,1]$ condition became invisible in both $g = [1\,3\,\bar{1}]$ and $g = [2\,2\,0]$ conditions, implying the contrast is caused by Shockley partial segments.

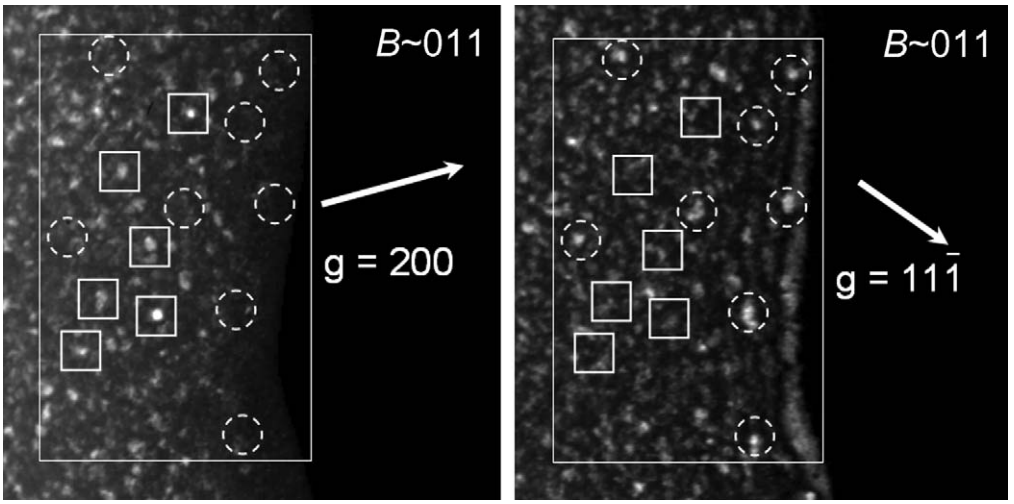

Fig. 3. Weak beam dark field images of the defect microstructures in cubic SiC irradiated at 800 °C to 7.7×10^{25} n/m^2. Note that the loops with a strong contrast in the [2 0 0] reflection (in solid squares) do not appear in the $[1\,1\,\bar{1}]$ reflection image, and vice versa (in dashed circles).

The microstructures for the case of irradiation by silicon ions are shown in Fig. 4 at a dose of 10 dpa. The micrographs in Fig. 4(A)–(C) were taken in a $B \sim [0\,1\,1]$ and $g = [2\,0\,0]$ condition. The ion irradiation at 800 °C produced defect structures very similar to that of neutron irradiation at the same temperature, comprising dislocation loops and smaller defects which are classified as black spot defects. The measured mean defect size in the ion-irradiated sample was slightly larger than that in the sample neutron-irradiated to 7.7×10^{25} n/m^2, due primarily to the presence of the larger loop population. On the contrary, a slightly finer dislocation loop microstructure in the ion-irradiated sample has been reported in a work involving a direct comparison of the ion- and neutron-irradiated materials at the same dose [40]. The total number density of the loops and black spot defects appeared to be higher for the case of ion irradiation than for neutron irradiation. This indicates that the difference in defect microstructure between ion- and neutron-irradiation at 800 °C was not in defect species but in defect number density.

At 1000 °C, the ion-irradiated microstructure was similar to that after irradiation at 800 °C, consisting of dislocation loops and black spot defects. The defect number density was apparently lower than at 800 °C and close to that caused by neutron irradiation at 800 °C to similar doses. The mean defect size was again similar to that for the case of ion irradiation at 800 °C. No streaks corresponding to the extra $\{1\,1\,1\}$ planes were found in the electron

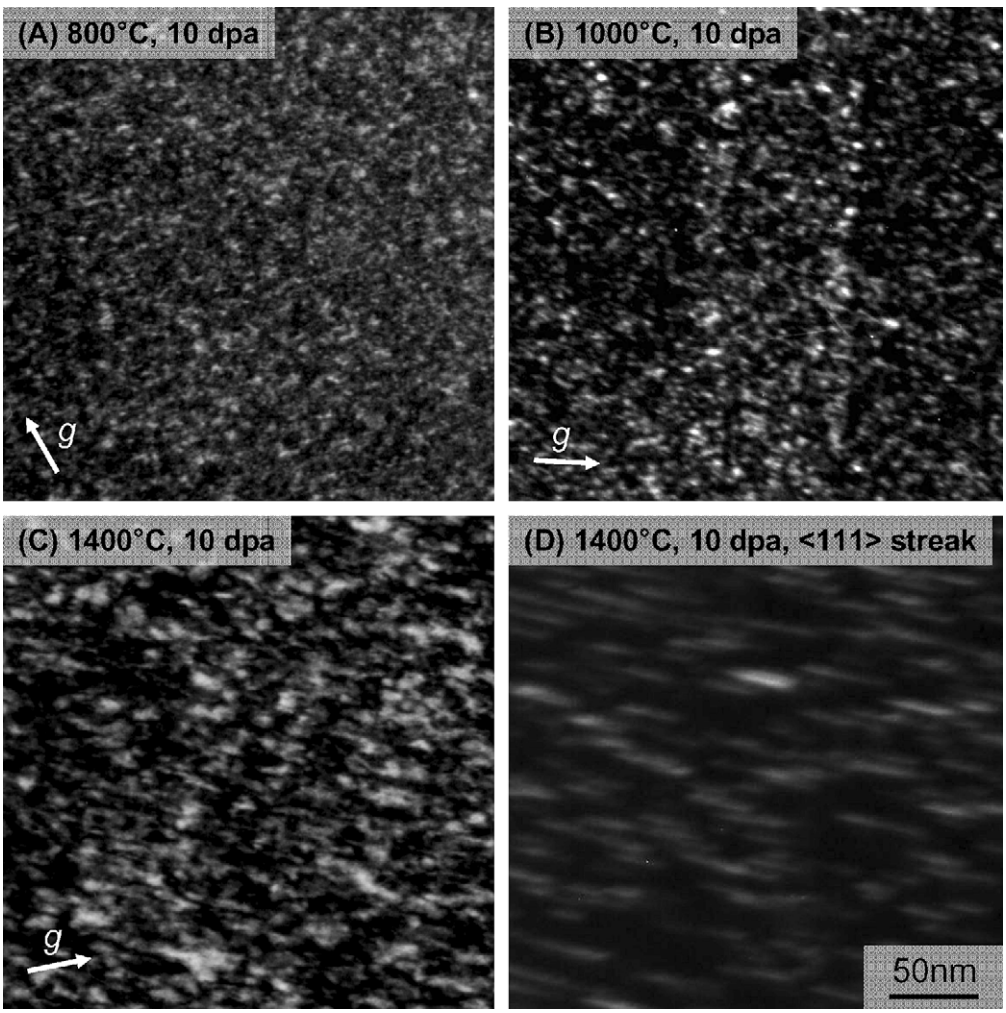

Fig. 4. Weak beam dark field images of the defect microstructures in cubic SiC irradiated to 10 dpa by Si^{2+} ions. Imaging conditions are as follows: (A–C) $B \sim [011]$, $g = [200]$; (D) $B \sim [011]$, $\langle 111 \rangle$ satellite streak image around $g = [200]$ reflection.

diffraction patterns obtained from the samples irradiated to 10 dpa at 800 °C and 1000 °C. Attempts of imaging by the assumed streak positions in the diffraction patterns revealed only the presence of twin boundaries. Therefore, the visible defect clusters are not Frank faulted loops.

The dominant features produced by ion-irradiation to 10 dpa at 1400 °C could be clearly identified as dislocation loops. These loops were much larger than those observed after irradiation at lower temperatures and appeared well oriented on the {1 1 1} planes. Streaks caused by the extra {1 1 1} planes were clearly observed in the electron diffraction pattern. The imaging by the streaks revealed Frank faulted loops, as shown in Fig. 4(D).

Fig. 5 shows the evolution of dislocation microstructure with the increasing fluence at 1400 °C. As seen in Fig. 5(A), the defect clusters become visible in TEM at 2 dpa as tiny black spot defects and small dislocation loops. These small dislocation loops do not have a stacking fault. At 10 dpa, the dislocation structure becomes primarily Frank faulted loops, but still the black spot defects and the smaller non-faulted loops are present (Fig. 5(B)). By 30 dpa, the Frank faulted loops grow to larger sizes and the black spot defects and the small non-faulted loops disappear (Fig. 5(C)). As the fluence exceeds ~100 dpa, the loops grow into dislocation network, which still involves loop-like segments at ~200 dpa, as seen in Fig. 5(D).

In Fig. 6, micrographs with the underfocused cavity images of the ion-irradiated samples are presented. These cavities are believed to be voids produced by the irradiation. Cavities were not

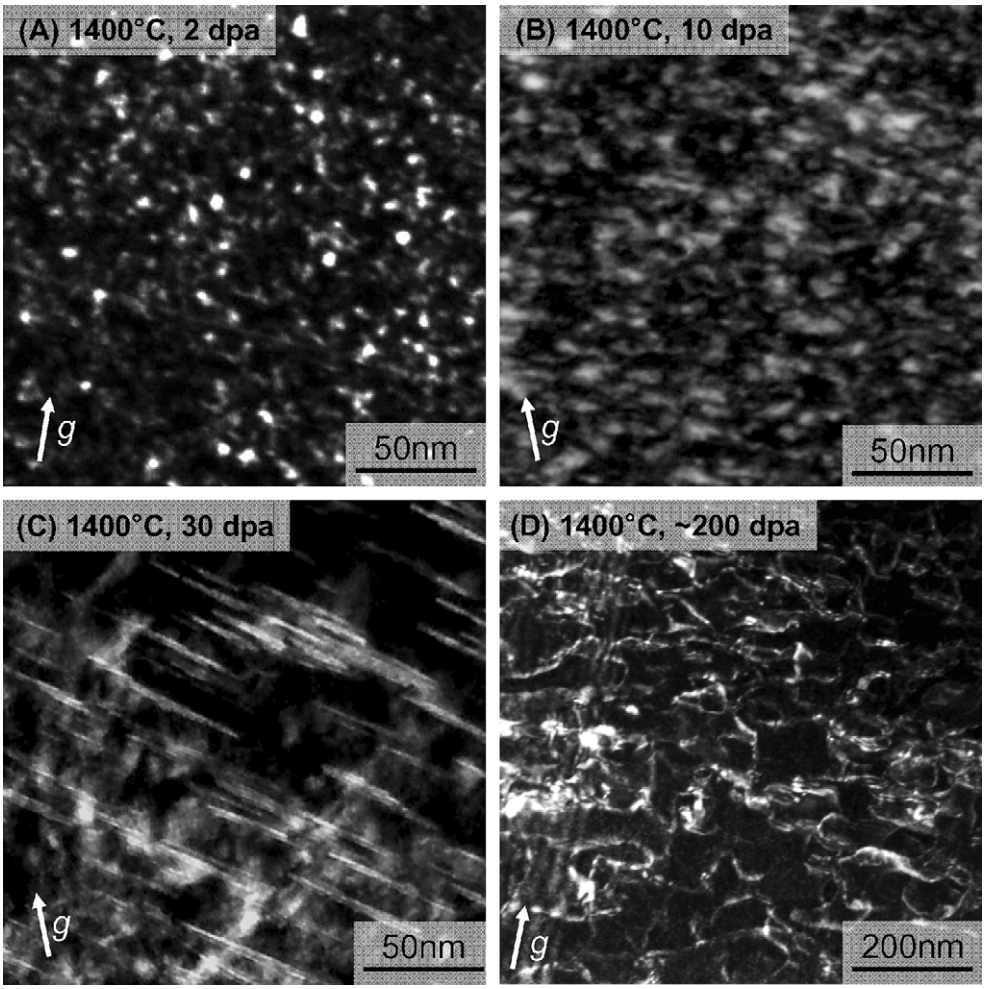

Fig. 5. Dose dependent evolution of dislocation microstructures in cubic SiC irradiated by Si^{2+} ions at 1400 °C. Imaging conditions are $B \sim [0\,1\,1]$, g in parallel to $[0\,1\,\bar{1}]$.

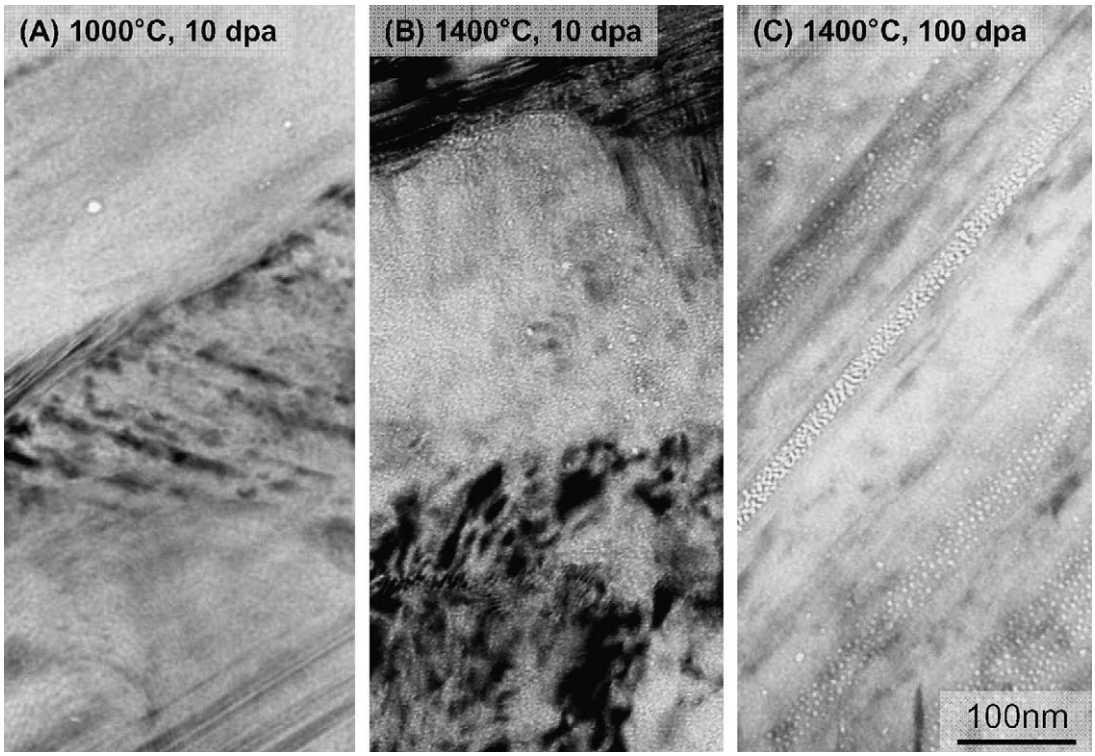

Fig. 6. Cavity microstructures in cubic SiC irradiated by Si^{2+} ions.

found in samples irradiated at 800 °C. After irradiation at 1000 °C, cavities were produced very sparsely. Fig. 6(A) is not representative of the cavity microstructure after irradiation at 1000 °C in terms of the number density. Such cavities were found only on grain boundaries at 1000 °C and 10 dpa, although that is not clearly seen in Fig. 6(A).

The cavities were more abundantly observed in samples ion-irradiated at 1400 °C. At 10 dpa the cavities were produced only on grain boundaries and stacking faults throughout the thin foil examined. Fig. 6(B) represents the cavity microstructure in that condition to some extent. The cavity number density increased dramatically by a dose of 30 dpa, due mainly to the extensive cavity nucleation on twin boundaries. By 100 dpa at 1400 °C, as seen in Fig. 6(C), the cavities had become more abundant. The cavity nucleation was still limited on stacking faults and grain/subgrain boundaries, and most of the cavities were found to be aligned flat on twin boundaries because of the much higher density for twin boundaries than the other types of planar boundaries. Cavities on the grain boundaries were generally larger in size and more separated each other. The cavity number density and mean radius measured within the cavity-rich regions are summarized in Table 1. The cavity number density averaged over the entire specimen would be much lower. The volumetric average swelling by cavities is estimated to be <1% at 100 dpa and 1400 °C.

4. Discussion

4.1. Dislocation loop evolution

Defect clusters which have collapsed into dislocation loops have been reported in cubic SiC neutron-irradiated at temperatures higher than ~600 °C [26,41–44]. Many of the dislocation loops have been identified or speculated to be $a/3\langle 1\,1\,1\rangle$ Frank faulted loops of interstitial type [33,42]. The result of the present work is consistent with those reports in that dislocation loops were observed at 800 °C and defect clusters appearing as black spots were observed at 300 °C.

In Fig. 7, the mean loop radius and the number density from both the present work and the literature are plotted against irradiation temperature. The numbers placed adjacent to the data points indicate the fast neutron fluence ($\times 10^{25}$ n/m^2) for the case

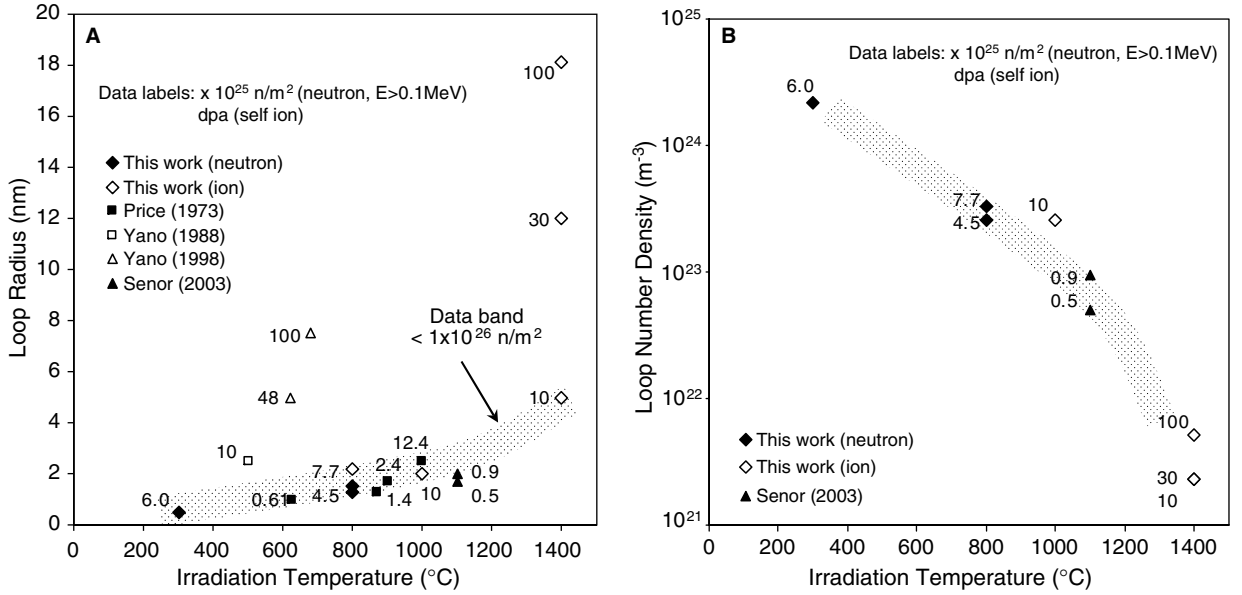

Fig. 7. Irradiation temperature dependence of dislocation loop radius (A) and number density (B) in irradiated cubic SiC. The data labels indicate fluences in 10^{25} n/m^2 ($E > 0.1$ MeV) for neutron irradiation and dpa for ion irradiation. All data are from neutron-irradiated specimens except where indicated otherwise.

of neutron irradiation and the damage level in dpa for the case of ion irradiation. As seen by the data band in Fig. 7(A), the mean loop radius increases with increasing irradiation temperature when compared for the fluence of $<\sim 1 \times 10^{26}$ n/m^2. This trend is inconsistent with the data compilation by Senor, in which a negative temperature dependence of the loop size is presented [44]. That happened probably by ignoring the potential strong fluence effect on the loop growth implied by the data points at high fluences [43]. Furthermore, the neutron fluence dependence of the loop microstructures has previously been based on the examination of materials irradiated in several different reactors in which the irradiation temperature control has not been reliable. The irradiation effects, including the dislocation loop growth, at fluences beyond 1×10^{26} n/m^2 in the lattice swelling temperature regime needs to be further studied by experiments in which the irradiation temperature is well-maintained.

The other question about the dislocation loops is their nature. Price reported that the small (2–5 nm in diameter) loops developed by irradiation to 0.6–0.9×10^{25} n/m^2 at 625 °C and to 2.4×10^{25} n/m^2 at 900 °C are presumably Frank loops [26]. Yano identified the larger (~15 nm) loops developed by irradiation to 1.0×10^{27} n/m^2 at ~640 °C primarily as the $a/3\langle 1\,1\,1\rangle$ Frank loops of interstitial type [42]. In the present work, Frank faulted loops with mean diameters of 13–36 nm were observed in samples irradiated by Si^{2+} ions to 30–100 dpa at 1400 °C.

On the other hand, the detailed Burgers vector analysis and identification of nature of defect clusters which are possibly dislocation loops were not performed because of the small sizes in many previous studies [44–46]. In the present work, electron diffraction patterns taken from the neutron irradiated samples did not show any detectable streak, indicating that the Frank faulted loops are not the dominating defects. In the specimen irradiated to 7.7×10^{25} n/m^2 at 800 °C, many of the relatively large loops seen in the reflection vector of $[2\,0\,0]$ disappeared with the reflection vector of $[1\,1\,\bar{1}]$ and vice versa. These loops are apparently not Frank faulted loops with $a/3\langle 1\,1\,1\rangle$ Burgers vectors. Further visibility analysis with different reflection vectors did not explicitly determine the loop identity but indicated that some of the loops have segments with Burgers vectors parallel to $\langle 1\,1\,0\rangle$. These loops are potentially be $a/2\langle 1\,1\,0\rangle$ loops, as reported by Stevens [47]. Therefore, it is concluded that at least two different kinds of dislocation loops, namely $a/3\langle 1\,1\,1\rangle$ Frank faulted loops and the other type which might be $a/2\langle 1\,1\,0\rangle$ perfect loops, are produced in cubic SiC under irradiation. It is likely that the loops prefer the configuration of the Frank

faulted loops due to the very small stacking fault energy of ~0.1 mJ/m^2 in cubic SiC [48], while smaller clusters tend to maintain the forms of other types of three-dimensional or planar defects at low doses and low temperatures. The reasons for the lack of energetically preferred Frank loops at relatively low temperatures presumably include the lack of thermal-spike phase during the cascade process in SiC as pointed out by Gao and Weber [49], high migration energy (~1.5 eV) for Si interstitials [50,51], and stoichiometric constraint for the formation of Frank loops.

From this work, it was also demonstrated that a dislocation network is developed in cubic SiC through the loop-loop and loop-network interactions at 1400 °C. Carter et al., reported the evolution of $a/2\langle 1\,1\,0\rangle$ perfect dislocations, and $a/3\langle 1\,1\,1\rangle$ Frank and $a/6\langle 1\,1\,2\rangle$ Shockley partial dislocations in cubic SiC crept at 1400–1700 °C [52]. Therefore, it is possible that the Frank faulted loops develop into dislocation network consisting primarily of $a/2\langle 1\,1\,0\rangle$ dislocations through the production of Shockley partials, as is common in fcc metals with small stacking fault energy [53]. Also, the large (50–100 nm in diameter) dislocation loops seen in heavily ion-irradiated samples were often highly irregular-shaped and not lying on single {1 1 1} planes anymore. This suggests that the Frank loops in cubic SiC tend to unfault themselves when excessively grown in size due to the change of energy hierarchy with cluster size. The interactions associated with the unfaulted loops are additional potential mechanisms for the dislocation network development. Future work will involve the determination of the nature of the network dislocations.

4.2. Cavity swelling

Formation of matrix voids has been reported by Price under neutron irradiation to 4.3×10^{25} n/m^2 at 1250 °C and at higher doses at higher temperatures [26]. In that work, voids were not observed after neutron irradiation to 1.24×10^{26} n/m^2 at 1000 °C. Senor reported the lack of void production after neutron irradiation to 0.9×10^{25} n/m^2 at 1100 °C but the production of matrix voids after subsequent annealing at 1500 °C for 1 h [44]. These observations indicate that the temperature regime for void swelling starts between 1100 and 1250 °C for neutron fluences in the order of 10^{25} n/m^2. The annealing experiment by Senor showed the limited mobility of vacancies at 1100 °C had prohibited the production of visible (by TEM) voids [44]. On the other hand, positron annihilation and electron paramagnetic resonance studies [54,55] have shown that the silicon vacancy in cubic SiC becomes mobile at 800–900 °C. Therefore, it is likely that the low temperature end of the void swelling regime comes down below 1100 °C as the neutron fluence increases.

In the self-ion irradiation experiment, voids in both the matrix and at grain boundaries were produced after 10 dpa at 1400 °C, while only sparsely distributed grain boundary voids were found in the sample irradiated to the same fluence at 1000 °C. In dual (and triple)-beam ion irradiation experiments, in which the self-ions and helium ions (and protons) are irradiated simultaneously, cavities were abundantly produced both in the matrix and on the grain boundaries after irradiation to 10 dpa at temperatures of 1000 °C or higher [56,57]. These indicate that the abundant production of the visible cavities have occurred by 10 dpa through the migration of vacancies at 1000 °C. A major difference between neutron irradiation in nuclear reactors and ion irradiation is the displacement damage rate. The damage rate for neutron irradiation in this work was $\sim5\times10^{-7}$ dpa/s, while that for ion irradiation was $\sim1\times10^{-3}$ dpa/s. According to a theory of displacement damage rate effect, temperature ranges for the irradiation-induced phenomena which are controlled by thermally activated processes shift toward lower temperatures when damage rate increases [58]. Hence, void swelling by neutron irradiation to high fluences may occur at temperatures lower than 1000 °C. However, the swelling rate at such temperatures would be quite low, because of the domination of point defect annihilation through the in-matrix recombination.

4.3. Mapping microstructural evolution

Fig. 8 summarizes the evolution of irradiation-produced microstructural features in cubic SiC under neutron and self-ion irradiation. At low temperatures and low fluences, the dominating feature is the black spot defect, which may be small interstitial clusters in various configurations. As the temperature and/or fluence increase, the black spot defects may become dislocation loops which are visible in TEM. Further increases in temperature and/or fluence promotes the development of Frank faulted loops. These transitions are probably due to the dependence of the cluster stability in various configurations on temperature and the size. Because of the very small stacking fault energy for cubic SiC,

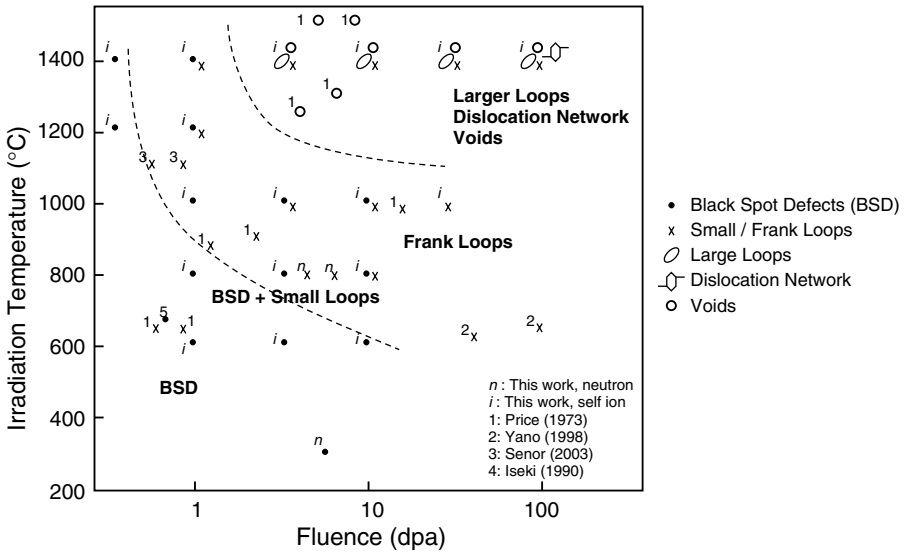

Fig. 8. Summary of the microstructural development in cubic SiC during neutron and self-ion irradiation.

Frank loops should be energetically the most preferred configuration for clusters with small sizes [59]. Therefore, the gradual transition of tiny interstitial clusters in irregular shapes, which might have been formed in relation to displacement cascade, into Frank loops could be expected. The Frank loops unfault by themselves or by interacting with dislocations during further growth, and eventually develop into network dislocations.

It is interesting to note the similarity of SiC with some of the fcc alloys in that the black spots and the Frank loops dominate at $<\sim 0.5T_{s,m}$ ($T_{s,m}$: sublimation or melting temperature) and the dislocation network develops at $>\sim 0.5T_{s,m}$. Significant void formation occurs at temperatures substantially higher than 1100 °C ($\sim 0.45T_s$), again similar to the behavior of fcc metals and alloys that develop large void swelling at $0.45–0.5T_m$.

The temperature–fluence regime for the large loops and network dislocation development coincides with that for void formation. One possible cause of this overlap of microstructural regimes is the void formation and growth due to the vacancy supersaturation caused by a dislocation bias mechanism, which is common in metallic systems [60].

4.4. Low temperature swelling

As introduced earlier, low temperature swelling of crystalline SiC is the isotropic expansion that occurs during irradiation at below ~1000 °C. The magnitude of low temperature swelling exhibits monotonic and negative irradiation temperature dependence and tends to saturate by a certain fluence, depending on temperature, of typically a few dpa [25]. The magnitude of linear swelling generally coincides very well with the magnitude of average lattice expansion as measured by the X-ray diffractometry (XRD) [61]. By annealing at temperatures higher than the irradiation temperature, the low temperature swelling recovers to approach to the magnitude of the equilibrium swelling by irradiation at the annealing temperature. During annealing, the macroscopic swelling magnitude again corresponds to the lattice expansion measured by XRD very well [61]. The lattice expansion and recovery behaviors are similar in cubic and hexagonal SiC, except that hexagonal SiC exhibits slightly anisotropic recovery [62].

A kinetic modeling of the low temperature swelling was first attempted by Balarin [63]. In that work, isolated point defects were assumed to be the source of the swelling. Even when a variety of formation and activation energies for point defects in different configurations [64,65], the model does not explain the nearly-linear temperature dependences of the swelling and the annealing behaviors.

Later, Huang and Ghoniem [66] and Ryazanov et al. [67], proposed models based on an assumption that Frank interstitial loops were responsible for the swelling. In order to account for the temperature dependence of swelling, the former relies on the

proposed exchange mechanism of C and Si interstitials in relation to the stoichiometry constraint for the Frank loops and their cascade resolution [66]. The latter proposed a model involving the growth of Frank interstitial loops by charge interactions [67]. Both models succeeded in accounting for some aspects of the experimentally observed low temperature swelling behavior. However, the total loop volume estimated from the experimental observation is usually low by one order of magnitude compared to the macroscopic volume change. For example, the visible loop volume in the specimen neutron-irradiated at 800 °C to 4.5×10^{25} n/m^2 is estimated to be 0.04%, whereas the measured swelling of the identical sample was ~0.9% [10]. Also, excess volumes for vacancies in cubic SiC are very small [32]. Therefore, the contribution of the visible interstitial loops and the corresponding amount of vacancies to the observed swelling should not be very significant.

The contribution by the interstitial clusters which are not sufficiently visible in TEM to the low temperature swelling of SiC is a strong possibility, by eliminating vacancies and Frank loops as discussed above. According to the molecular dynamics simulation by Li et al., using the Tersoff potential, excess volume for the Si interstitial can be tremendously large, reaching 3–4 times the atomic volume (Ω) [32]. Also, the excess volume for the C interstitial can be as large as ~1.5 Ω. The relaxation volumes per defect for the small clusters should decrease as the cluster size increases, starting from the excess volume for the isolated interstitials. The higher number density of the smaller interstitial clusters should result in larger lattice expansion, thus the monotonic temperature dependence of swelling could be explained. Yano reports the recovery of the lattice expansion is reached at 480–650 °C for the very high (>~3×10^{26} n/m^2) neutron fluence, and that it is accompanied by the microstructural transition from black spot defects to well-developed Frank loops [41]. This observation supports the hypothesis that small interstitial clusters including the visible black spot defects are primarily responsible for the lattice expansion at low temperatures.

5. Conclusions

Microstructures of polycrystalline beta-SiC irradiated by neutrons and self-ions were examined by TEM.

At relatively low temperatures (<~ 800 °C) where substantial low temperature swelling and thermal conductivity degradation occur, irradiation-produced defect features visible in TEM were small dislocation loops and black spot defects. The majority of the small dislocation loops did not appear to be faulted. The loops and black spot defects coarsened as the irradiation temperature increased, although the temperature dependence of defect size and density was mild. The neutron and ion irradiation produced similar microstructures in spite of the large difference in damage rate between them. It was presumed that the primary contributors to the low temperature swelling are the small interstitial clusters and the contributions from the dislocation loops and isolated point defects are rather minor.

Substantial information and insights were provided by the ion irradiation experiment with regard to the microstructural development at higher (>~1000 °C) temperatures. It was demonstrated that the initially produced black spot defects and tiny dislocation loops collapsed into Frank faulted loops at intermediate fluences and finally developed into a dislocation network at very high fluences. The dislocation loops appeared significantly coarser as either the irradiation temperature or fluence increased. Evolution of the dislocation microstructures appeared similar to that in some fcc metals and alloys. Cavities were formed only on (sub-) grain boundaries and stacking faults at >1000 °C. At 1400 °C, all the pre-existing stacking faults were heavily decorated with the high density cavities after irradiation to >30 dpa. However, the swelling by cavities was still small. It should be noted that the understanding of neutron-ion correlation is severely lacking in the high temperature regime. Substantial dose rate effect is anticipated at high temperatures, where the strong temperature dependence of microstructural evolution was observed.

Acknowledgements

This research was sponsored by the Office of Fusion Energy Sciences, US Department of Energy under contract DE-AC05-00OR22725 with UT-Battelle, LLC, the 'JUPITER-II' US-Department of Energy/Japanese Ministry of Education, Culture, Sports, Science and Technology (MEXT) collaboration for fusion material system research, and the IVNET GFR Program supported by MEXT, Japan.

References

[1] R.J. Price, Nucl. Technol. 35 (1977) 320.
[2] G.O. Hayner et al., Next Generation Nuclear Plant Materials Research and Development Program Plan, INEEL/EXT-04-02347 Revision 1, Idaho National Engineering and Environmental Laboratory, Idaho Falls, 2004.
[3] A. Kohyama, T. Hinoki, T. Mizuno, T. Kunugi, M. Sato, Y. Katoh, J.S. Park, R& D of Advanced material systems for reactor core component of gas cooled fast reactor, in: Proceedings of the International Congress on Advances in Nuclear Power Plants, 15–19 May 2005, Seoul.
[4] M. Konomura, T. Mizuno, T. Saigusa, Y. Ohkubo, A Promising Gas-Cooled Fast Reactor Concept and Its R&D Plan, in: GLOBAL 2003, 16–20 November 2003, New Orleans.
[5] B. Riccardi, L. Giancarli, A. Hasegawa, Y. Katoh, A. Kohyama, R.H. Jones, L.L. Snead, J. Nucl. Mater. 329–333 (2004) 56.
[6] L. Giancarli, H. Golfier, S. Nishio, R. Raffray, C. Wong, R. Yamada, Fusion Eng. Des. 61&62 (2002) 307.
[7] M. Abdou, D. Sze, C. Wong, M. Sawan, A. Ying, N. Morley, Fusion Sci. Technol. 47 (2005) 475.
[8] R.J. Price, G.R. Hopkins, J. Nucl. Mater. 108&109 (1982) 732.
[9] M.C. Osborne, J.C. Hay, L.L. Snead, D. Steiner, J. Am. Ceram. Soc. 82 (1999) 2490.
[10] L.L. Snead, R. Scholz, A. Hasegawa, A.F. Rebelo, J. Nucl. Mater. 307–311 (2002) 1141.
[11] S. Nogami, A. Hasegawa, L.L. Snead, J. Nucl. Mater. 307–311 (2002) 1163.
[12] G. Newsome, L.L. Snead, T. Hinoki, Y. Katoh, J. Nucl. Mater., submitted for publication.
[13] Y. Katoh, L.L. Snead, J. ASTM Int. 2 (2005) 12377.
[14] W. Dienst, J. Nucl. Mater. 191–194 (1992) 555.
[15] W. Dienst, J. Nucl. Mater. 211 (1994) 186.
[16] W. Dienst, H. Zimmermann, J. Nucl. Mater. 212–215 (1994) 1091.
[17] L.L. Snead, Y. Katoh, A. Kohyama, J.L. Bailey, N.L. Vaughn, R.A. Lowden, J. Nucl. Mater. 283–287 (2000) 551.
[18] T. Hinoki, L.L. Snead, Y. Katoh, A. Hasegawa, T. Nozawa, A. Kohyama, J. Nucl. Mater. 307–311 (2002) 1157.
[19] Y. Katoh, A. Kohyama, T. Hinoki, L.L. Snead, Fusion Sci. Technol. 44 (2003) 155.
[20] T. Nozawa, T. Hinoki, L.L. Snead, Y. Katoh, A. Kohyama, J. Nucl. Mater. 329–333 (2004) 544.
[21] J.I. Bramman, A.S. Fraser, W.H. Martin, J. Nucl. Eng. 25 (1971) 223.
[22] R. Blackstone, E.H. Voice, J. Nucl. Mater. 39 (1971) 319.
[23] R.J. Price, Nucl. Technol. 16 (1972) 536.
[24] J.E. Palentine, J. Nucl. Mater. 61 (1976) 243.
[25] Y. Katoh, H. Kishimoto, A. Kohyama, J. Nucl. Mater. 307–311 (2002) 1221.
[26] R.J. Price, J. Nucl. Mater. 46 (1973) 268.
[27] J.C. Corelli, J. Hoole, J. Lazzaro, C.W. Lee, J. Am. Ceram. Soc. 66 (1983) 529.
[28] M. Rohde, J. Nucl. Mater. 182 (1991) 87.
[29] L.L. Snead, J. Nucl. Mater. 329–333 (2004) 524.
[30] H. Huang, N.M. Ghoniem, J.K. Wong, M.I. Baskes, Model. Simul. Mater. Sci. Eng. 3 (1995) 615.
[31] F. Gao, W.J. Weber, M. Posselt, V. Belko, Phys. Rev. B 69 (2004) 245205.
[32] J. Li, L. Porter, S. Yip, J. Nucl. Mater. 255 (1998) 139.
[33] R.J. Price, J. Nucl. Mater. 48 (1973) 47.
[34] R. Scholz, J. Nucl. Mater. 258–263 (1998) 1533.
[35] R. Scholz, G.E. Youngblood, J. Nucl. Mater. 283–287 (2000) 372.
[36] R. Scholz, R. Mueller, D. Lesueur, J. Nucl. Mater. 307–311 (2002) 1183.
[37] A. Kohyama, Y. Katoh, M. Ando, K. Jimbo, Fusion Eng. Des. 51&52 (2000) 789.
[38] A. Kohyama, Y. Katoh, K. Jimbo, Mater. Trans. 45 (2004) 51.
[39] J. Ziegler, Particle interactions with matter. Available from: <http://www.srim.org/>.
[40] S. Kondo, Y. Katoh, K.H. Park, A. Kohyama, Am. Ceram. Soc. 5 (2004) 229.
[41] T. Yano, T. Suzuki, T. Maruyama, T. Iseki, J. Nucl. Mater. 155–157 (1988) 311.
[42] T. Yano, T. Iseki, Philos. Mag. A 62 (1990) 421.
[43] T. Yano, H. Miyazaki, M. Akiyoshi, T. Iseki, J. Nucl. Mater. 253 (1998) 78.
[44] D.J. Senor, G.E. Youngblood, L.R. Greenwood, D.V. Archer, D.L. Alexander, M.C. Chen, G.A. Newsome, J. Nucl. Mater. 317 (2003) 145.
[45] T. Iseki, T. Maruyama, T. Yano, T. Suzuki, J. Nucl. Mater. 170 (1990) 95.
[46] S. Kondo, T. Hinoki, A. Kohyama, Mater. Trans. 46 (2005) 1923.
[47] R. Stevens, Phil. Mag. 25 (1972) 523.
[48] U. Kaiser, I.I. Khodos, Philos. Mag. A 82 (2002) 541.
[49] F. Gao, W.J. Weber, Phys. Rev. B 63 (2000) 054101-1-7.
[50] W.J. Weber, W. Jiang, S. Thevuthasan, Nucl. Instrum. and Meth. B 175–177 (2001) 26.
[51] F. Gao, W.J. Weber, M. Posselt, V. Belko, Phys. Rev. B 69 (2004) 245205-1-5.
[52] C.H. Carter Jr., R.F. Davis, J. Bentley, J. Am. Ceram. Soc. 67 (1984) 732.
[53] D.S. Gelles, in: M.F. Ashby, R. Bullough, C.S. Hartley, J.P. Hirth (Eds.), Dislocation Modelling of Physical Systems, Pergamon, New York, 1980, p. 158.
[54] H. Itoh, H. Hayakawa, I. Nashiyama, E. Sakuma, J. Appl. Phys. 66 (1989) 4529.
[55] A. Kawasuso, H. Itoh, N. Morishita, T. Ohshima, I. Nashiyama, S. Okada, H. Okumura, S. Yoshida, Appl. Phys. A 67 (1998) 209.
[56] S. Kondo, K.H. Park, Y. Katoh, A. Kohyama, Fusion Sci. Technol. 44 (2003) 181.
[57] A. Hasegawa, S. Nogami, S. Miwa, K. Abe, T. Taguchi, N. Igawa, Fusion Sci. Technol. 44 (2003) 175.
[58] L.K. Mansur, J. Nucl. Mater. 78 (1978) 156.
[59] S.J. Zinkle, L.E. Seitzman, W.G. Wolfer, Philos. Mag. A 55 (1987) 111.
[60] L.K. Mansur, in: G.R. Freeman (Ed.), Kinetics of Nonhomogeneous Processes, John Wiley, Inc., 1987.
[61] T. Suzuki, T. Yano, T. Mori, H. Miyazaki, T. Iseki, Fus. Technol. 27 (1995) 314.
[62] Y. Pramono, M. Imai, T. Yano, J. Nucl. Sci. Technol. 40 (2003) 531.
[63] M. Balarin, Phys. Status Solidi 11 (1965) K67.
[64] F. Gao, E.J. Bylaska, W.J. Weber, L.R. Corrales, Phys. Rev. B 64 (2001) 245208-1-7.
[65] F. Gao, W.J. Weber, J. Appl. Phys. 94 (2003) 4348.
[66] H. Huang, N. Ghoniem, J. Nucl. Mater. 250 (1997) 192.
[67] A.I. Ryazanov, A.V. Klaptsov, A. Kohyama, H. Kishimoto, J. Nucl. Mater. 307–311 (2002) 1107.